# Hardness and Microstructure Characterization of Hardfacing Alloys Deposited by The Shielded Metal Arc Welding (SMAW) on AISI 1045 Medium Carbon Steel

**Basyirun Basyirun[1]\*, Muhammad Hasnan Habib[1], Deni Fajar Fitriyana[1], Muhammad Irfan Nuryanta[1], Januar Parlaungan Siregar[2], Tezara Cionita[3], Natalino Fonseca Da Silva Guterres[4], Mateus De Sousa Da Silva[4]**

[1] Department of Mechanical Engineering, Faculty of Engineering,
    Universitas Negeri Semarang, Semarang 50229, INDONESIA

[2] Faculty of Mechanical & Automotive Engineering Technology,
    Universiti Malaysia Pahang, Pekan 26600, Pahang, MALAYSIA

[3] Faculty of Engineering and Quantity Surveying,
    INTI International University, Nilai 71800, Negeri Sembilan, MALAYSIA

[4] Department of Mechanical Engineering,
    Dili Institute of Technology, Aimeti Laran Street, Dili, TIMOR LESTE

*Corresponding Author: basyirun@mail.unnes.ac.id
DOI: https://doi.org/10.30880/ijie.2024.16.05.008

## Abstract

A ring frame is a machine used for yarn production in the textile industry. Continuous use of the machine results in wear on the shaft timing pulley on the ring frame machine. To improve this condition, repairs are needed, one of which uses the hardfacing method. This study aims to determine the effect of hardfacing on the microstructure and hardness of the shaft timing pulley made from AISI 1045. The hardfacing process used the shielded metal arc welding (SMAW) method with welding current variations of 115 A, 125 A, 135 A, 145 A, and 155 A. In this study, the electrode used was AWS A5.1 E7018 with a diameter of 3.2 mm. The hardfacing product obtained was then finished with a lathe to produce a shaft with a final diameter of 30 mm. In this study, microstructure and hardness tests were carried out on specimens before and after finishing. The results of this study showed that an increase in current caused an increase in the number of pearlite phases in the weld metal and HAZ (heat-affected zone) areas. While in the base metal, the increase in current increased the number of ferrite phases. The highest hardness value was found in specimens that were hardfaced with a current of 145 A. However, the hardness of the hardfacing layer will decrease with the use of currents greater than 145 A. The hardness of the specimens with hardfacing treatment at a current of 145 A resulted in hardness in the weld metal, HAZ, and base metal of 225 HV, 209 HV, and 203 HV, respectively. After the finishing process, the weld metal, HAZ, and base metal in this specimen produced a hardness of 225 HV, 217 HV, and 208 HV, respectively.

## 1. Introduction

A ring frame is a machine used in the textile industry that consists of a number of spindles to measure the production capacity of a capital [1]. On the machine, there is a shaft timing pulley which functions as a forwarder of rotation power from the motor to the next machine element. The shaft becomes a mechanical device component that is stationary and has the function of transmitting rotary motion and power [2], [3]. The problem that occurs in the Ring Frame machine is that the bearing that is directly connected to the shaft timing pulley is damaged due to vibration. When the bearing is damaged, while the rotating power of the shaft timing pulley is still there, it results in the two machine elements rubbing against each other so that the shaft timing pulley is eroded or worn (Fig. 1) [2], [3]. Therefore, it is necessary to take corrective action on the worn shaft parts, one of which is the hardfacing method.



**Fig. 1** *The wear of the shaft timing pulley on the ring frame machine*

Hardfacing is a surface processing technique through a welding process that involves adding a surface layer to the material that is harder and more wear-resistant than the base material. The main purpose is to improve the wear resistance of the base material [4]–[6]. Hardfacing involves the deposition of durable and abrasion-resistant material onto the outer layer of a component by techniques such as welding or thermal spraying. Its primary purpose is to minimize wear and tear. Hardfacing is employed for the initial application of new equipment and for restoring worn-out components. Hardfacing consumable materials can be utilized in several formats, including powder, hard welding rods or wires, and tubular rods or wires [7]. Hardfacing has been widely applied as a surface repair technique in various industries. In its application, the service life of components subjected to abrasive wear and corrosion can be extended by the deposition of a hard coating on components exposed to extreme conditions during operation [8], [9]. So hardfacing is considered an effective method to increase component life. As a result, there is growing interest in hardfacing and its applications. In its approach, hardfacing usually relies on applications that govern the selection of consumables, substrates, and deposition processes. The welding method is chosen because it can affect the dilution, fusion, microstructure, and hardness of the weld deposit [10], [11]. As a result, these methods and parameters can affect the hardfacing performance or the intended application of the structure and its components. In the experiment, that welding current, speed, and stand-off distance become the most important process factors [12]. On the other hand, several studies confirmed that welding factors and techniques showed a great influence on the microstructure and mechanical characteristics of hardfacing [13]. In Suharno's research (2023), to determine the effect of current on mechanical properties in conditions before and after welding, the effect of current variations of 110 A, 120 A, and 130 A on ASTM A36 steel with the SMAW method and E7016 electrode can affect microstructure, tensile strength, and hardness values. The result of this study shows that welding current has a significant effect on mechanical properties [14].

The main advantages of hardfacing include the restoration of worn-out components and the protection of new metal parts against metal erosion. Hard facing is mostly done to reduce expenses by refurbishing a worn metal element to a similar state as when it was new, which often costs just 25 to 75% of the price of the new component. Additionally, it significantly prolongs the lifespan of equipment by a factor of 30 to 300 while minimizing downtime and the need for spare parts inventories. Less costly base metals can also be used to manufacture hard-faced components [15]. However, there has been a lack of a comprehensive and systematic study examining the

application of hardfacing to address the damage and wear encountered by AISI 1045 shafts in ring frame machines. Hence, this work aims to evaluate the hardness and microstructure of hardfacing layers fabricated using shielded metal arc welding (SMAW) at various current levels, specifically 115 A, 125 A, 135 A, 145 A, and 155 A.

## 2. Materials and Methods

In this study, the shaft timing pulley was obtained from Primayudha Mandirijaya Ltd. with the chemical composition shown in Table 1. The results of the chemical content showed a carbon percentage of 0.457, making it clear that the material is classified as a type of medium carbon steel because the content is in the range of 0.30%−0.60% [16], [17]. AISI 1045 steel is a material that belongs to the medium carbon steel group and has a content in the range of 0.43%−0.50% and is a material commonly used in the manufacturing sector [18]−[21]. The raw material utilized in this study exhibited a hardness of 213.4 HV. After knowing the chemical content and requirements of the material, this study used AISI 1045 material in the form of a cylinder with a diameter of 29 mm and a length of 40 cm.

**Table 1** *Chemical content of shaft timing pulley*

| Element | C | Si | Mn | P | S | Cr | Mo | Ni | Cu | Fe |
|---------|------|------|-------|-------|-------|-------|------|-------|-------|-------|
| % | 0.457 | 0.24 | 0.856 | 0.036 | 0.011 | 0.098 | 0.01 | 0.052 | 0.065 | 98.15 |

The hardfacing process was carried out using the Shielded metal arc welding (SMAW) method using an ESAB machine type Warrior 500i CC/CV from ESAB Corporation, Montgomery County, USA.

This machine has a main voltage, frequency, and current of 380 - 575 V, 50/60 Hz, and 16 - 500 A respectively. The hardfacing process used AWS A5.1 E7018 model RD-718 electrode with NIKKO STEEL brand produced by Alam Lestari Unggul Ltd. This electrode has a Tensile Strength (kgf/mm$^2$) and yield point (kgf/mm$^2$) of 61.0 and 56.0 respectively. In this study, hardfacing on AISI 1045 type material was carried out in the 1G position with variations in the current use of 115 A, 125 A, 135 A, 145 A, and 155 A. AISI 1045 specimens that have been hardfaced, were finished using a lathe to produce a final diameter of 30 mm. The specimen codes used in this study are shown in Table 2.

**Table 2** *Parameters and specimen codes*

| No | Current (A) | Conditions | Specimen codes |
|----|-------------|------------------|----------------|
| 1 | 115 | Before Finishing | 115-1 |
| 2 | 125 | Before Finishing | 125-1 |
| 3 | 135 | Before Finishing | 135-1 |
| 4 | 145 | Before Finishing | 145-1 |
| 5 | 155 | Before Finishing | 155-1 |
| 6 | 115 | After Finishing | 115-2 |
| 7 | 125 | After Finishing | 125-2 |
| 8 | 135 | After Finishing | 135-2 |
| 9 | 145 | After Finishing | 145-2 |
| 10 | 155 | After Finishing | 155-2 |

Microstructure and hardness tests were conducted on AISI 1045 specimens before and after finishing. Microstructure testing using Lumenera Infinity 2-1 Digital CCD Microscope Camera from OEM-OPTICAL.COM, Danville, California, United States. Vickers hardness testing on specimens using Microhardness Tester Fm-800 from Future-Tech Corp., Kanagawa, Japan. This test is used to determine the strength, hardness, and ductility of the material [22]−[25]. This test uses a prism-shaped indenter with a diagonal between long and short of about 7 to 1 [26]. This hardness test is carried out in 3 areas, namely: base metal, HAZ, and weld metal. Each area was tested 3 times to produce 3 hardness values, then the average was calculated. The standard used in this hardness test is the AWS D8.9-97 standard, with an indenter speed of 200 μm/second, a constant pressure of 200 gf, and a pressing time of 10 seconds [27]. The results of the hardness value can be seen on the test machine monitor after the test process is complete.

## 3. Results and Discussion

Fig. 2 displays the microstructure of 115-1 specimen. The microstructure analysis reveals the presence of both ferrite and pearlite. Ferrite is denoted by regions that look white, whereas black regions indicate the presence of pearlite [28].

The weld metal area was dominated by ferrite and pearlite phases with a tight distribution (Fig. 2a). The quantity of the pearlite phase exceeds that of the ferrite phase. As a result, the weld metal area in 115-1 specimen becomes hard and brittle.
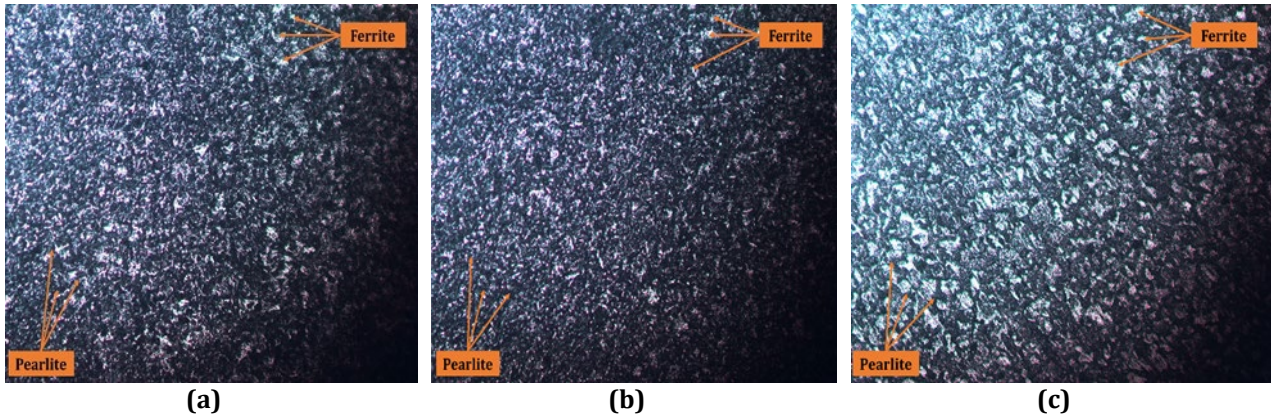


**(a)**      **(b)**      **(c)**

**Fig. 2** *Microstructure of the 115-1 specimen: (a) weld metal; (b) HAZ; (c) base metal*

Fig. 2b displays the HAZ area in the 115-1 specimen. Like the weld metal area, the heat-affected zone (HAZ) area contains two distinct phases: pearlite and ferrite. Nevertheless, the quantity of ferrite is greater than the area of the weld metal. The HAZ area has a dense distribution of phases, with a higher proportion of pearlite than ferrite, resulting in its hard and brittle characteristics. Fig 2c displays the microstructure of the base metal area. In the base metal area, ferrite is more common than pearlite in the microstructure, which makes it soft and malleable. Comparatively, considering the entire microstructure, the base metal region exhibits the least strength, followed by the weld metal and heat-affected zone (HAZ) regions.

A greater quantity of pearlite than the ferrite phase indicates that the steel underwent a gradual cooling process, which prolonged the diffusion of carbon atoms and subsequent formation of pearlite. The increase in pearlite content can result in increased hardness and increased brittleness. Pearlite contributes to an increase in hardness due to its composition, which includes around 12.5% cementite, a harder phase than ferrite. Pearlite is a two-phase substance consisting of cementite (12.5 wt%) and ferrite (87.5 wt%) arranged alternately [29]–[31]. The inclusion of cementite within the pearlite structure enhances the material's hardness. Thus, the material's hardness will escalate if pearlite surpasses ferrite in dominance [29]–[33]. Conversely, a soft and ductile substance is produced when ferrite dominates in comparison to the pearlite phase. Ferrite is a solid solution of carbon in iron, characterized by a body-centered cubic crystal structure. The carbon concentration of pearlite is reduced compared to cementite; the other phase found in pearlite. Ferrite imparts excellent ductility to the material, enabling it to undergo deformation and withstand plastic deformation without exhibiting brittle fracture [34], [35].
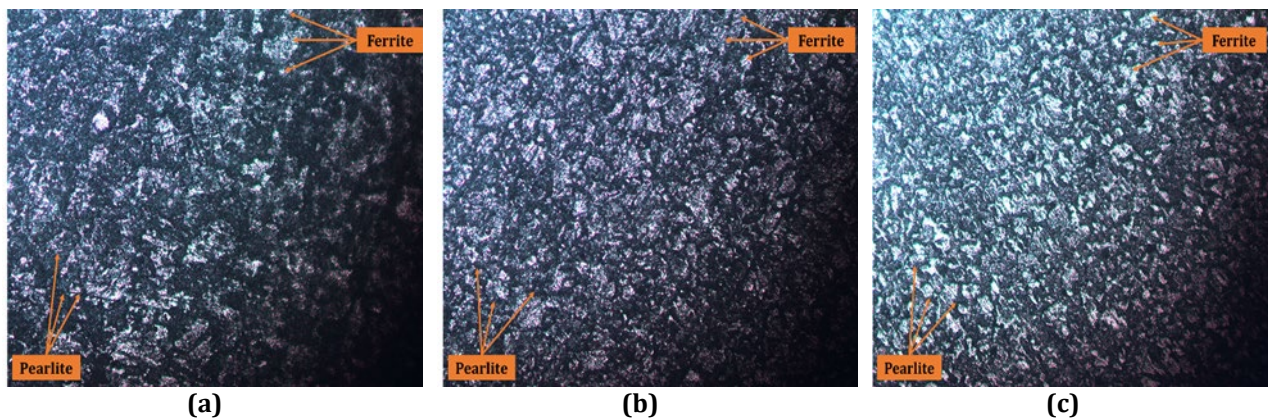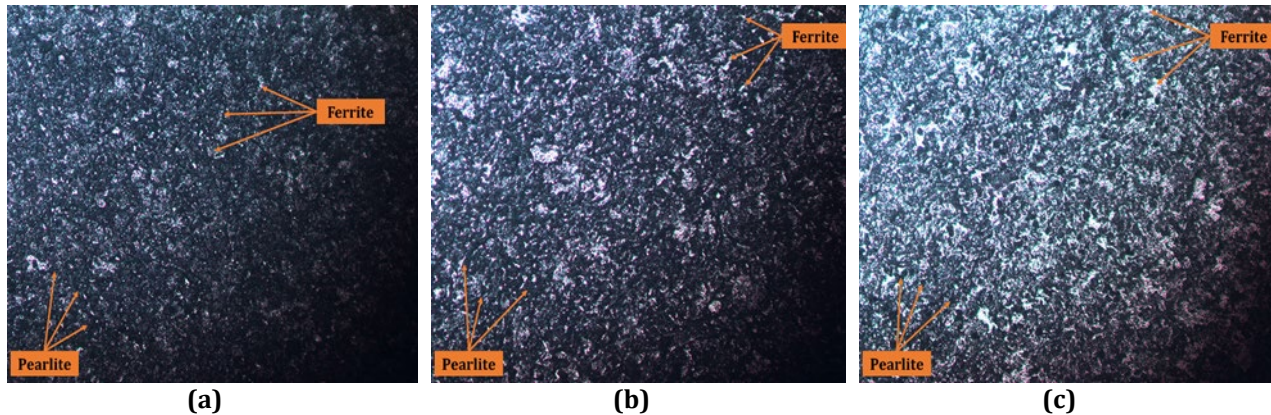


**(a)**      **(b)**      **(c)**

**Fig. 3** *Microstructure of the 125-1 specimen: (a) weld metal; (b) HAZ; (c) base metal*

The weld metal region in specimen 125 A-1 exhibits the presence of ferrite and pearlite phases, as depicted in Fig 3a. The pearlite phase is more prevalent than the ferrite phase in the weld metal. The ferrite phase, characterized by its bright white appearance, often contains a minimal quantity, in contrast to the pearlite phase. In the 125 A-1 specimens, the HAZ region revealed that the ferrite phase grains appear delicate, while the pearlite phase is slightly more prevalent (Fig.3b).
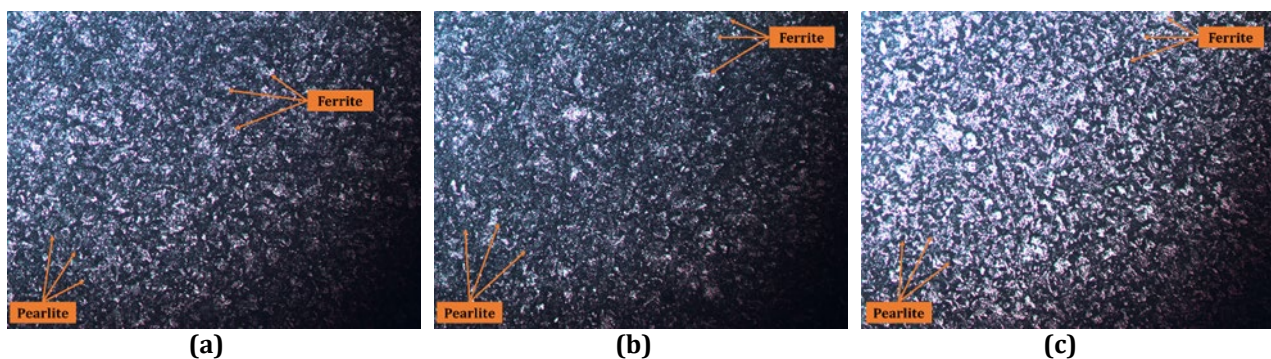
While the microstructure of the base metal region in the 125 A-1 specimen (Fig.3c) exhibits a uniform distribution of ferrite and pearlite phase grains. The results of this investigation reveal that the hardness of the base metal area is lower than the weld metal and HAZ areas.



**(a)**                                              **(b)**                                              **(c)**

**Fig. 4** *Microstructure of the 135-1 specimen: (a) weld metal; (b) HAZ; (c) base meta.*

Fig. 4a displays the microstructure images of the weld metal region in specimen 135-1. The distribution of the apparent ferrite phase in the weld metal is non-uniform and tends to be predominantly pearlite. A similar occurrence occurs in the HAZ region (Fig. 4b). Nevertheless, the quantity of ferrite present in the heat-affected zone (HAZ) is somewhat higher than that in the weld metal area, making the weld metal area comparatively harder and more susceptible to brittleness. The analysis of specimen 135-1 reveals that the ferrite phase is more prevalent than the pearlite phase in the base metal (Fig. 4c). The results indicate a reduction in the base metal's hardness due to the prevalence of ferrite. This occurs due to the enhanced presence of the pearlite phase, which contributes to the material's increased toughness, while the ferrite phase imparts softness and ductility.

The examination of specimen 145-1 reveals contrasting microstructures and phase quantities between the weld metal (Fig. 5a) and HAZ (Fig. 5b) areas. The weld metal and heat-affected zone (HAZ) contain a higher proportion of pearlite compared to ferrite. A higher quantity of ferrite in the Heat Affected Zone (HAZ) suggests a reduction in hardness relative to the weld metal region. The base metal microstructure image of specimen 145-1 demonstrates ferrite phases, which are slightly larger than pearlite (Fig. 5c). The results indicate a reduction in the base metal's hardness, attributed to the dominance of ferrite. This phenomenon arises from the heightened presence of the pearlite phase, which enhances the material's toughness, while the ferrite phase offers softness and ductility.
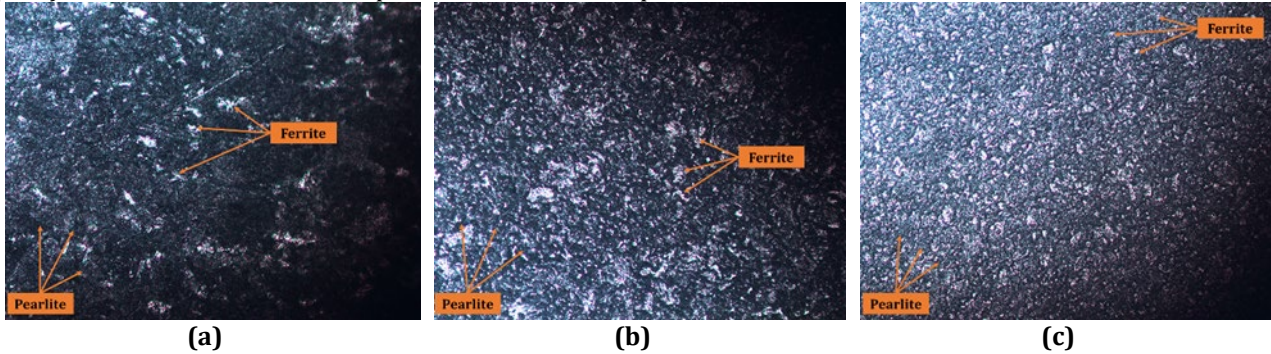


**(a)**                                              **(b)**                                              **(c)**

**Fig. 5** *Microstructure of the 145-1 specimen: (a) weld metal; (b) HAZ; (c) base metal*

The microstructure and number of phases in specimen 155-1 are different in the regions of the weld metal (Fig. 6a), and the heat-affected zone (HAZ) (Fig. 6b). The weld metal and HAZ regions exhibit more pearlite than ferrite. Nevertheless, a greater amount of ferrite was detected in the heat-affected zone (HAZ) compared to the area of the welded metal. The discrepancy elucidates that the weld metal region possesses a greater hardness level than the heat-affected zone (HAZ) area. Specimen 155-1's base metal microstructure image reveals a slightly

greater ferrite phase than pearlite (Fig. 6c). The findings indicate that the high ferrite level reduced the base metal's hardness.

Fig. 7 demonstrates the microstructure findings of specimen 115-2. The microstructure observed in the weld metal (Fig. 7a), heat-affected zone (Fig. 7b), and base metal (Fig. 7c) regions of specimen 115-2 exhibits variations in the quantity and arrangement of ferrite and pearlite phases. The areas of the weld metal, heat-affected zone (HAZ), and base metal exhibit the presence of ferrite and pearlite.



(a)　　　　　　　　　(b)　　　　　　　　　(c)

**Fig. 6** *Microstructure of the 155-1 specimen: (a) weld metal, (b) HAZ, and (c) base metal*

Nevertheless, the weld metal region shows a reduced quantity and diminished size of ferrite phases compared to the heat-affected zone (HAZ) and the base metal regions. In contrast to the weld metal area, the base metal and heat-affected zone (HAZ) areas exhibit a higher concentration and bigger size of ferrite phases. The weld metal area has a higher proportion of the pearlite phase, characterized by its brittle and hard characteristics. In the heat-affected zone (HAZ) and base metal regions, a higher concentration of ferrite was observed compared to the weld metal region. The presence of the pearlite phase in the heat-affected zone (HAZ) is reduced compared to the weld metal region. The weld metal area generally exhibits a significantly higher hardness value than the heat-affected zone (HAZ) and the base metal portions. This occurs due to the dominant presence of pearlite over ferrite in the weld metal region.



(a)　　　　　　　　　(b)　　　　　　　　　(c)
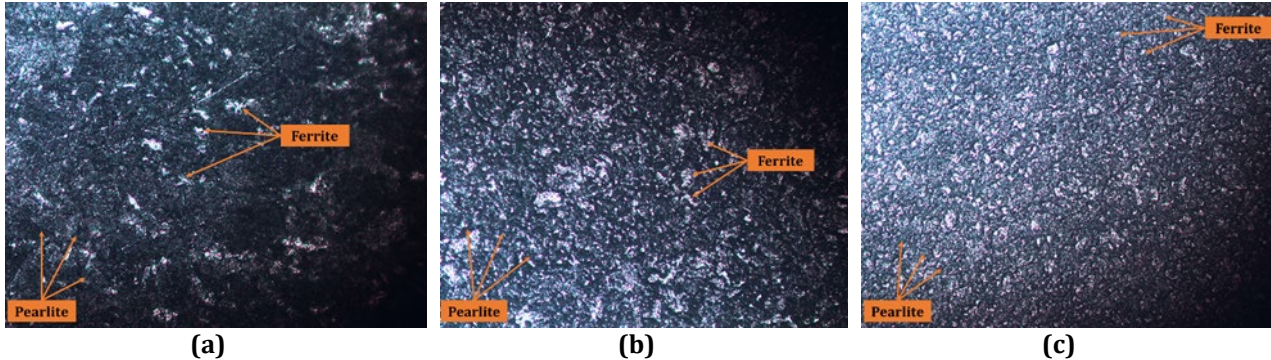
**Fig. 7** *Microstructure of the 115-2 specimen: (a) weld metal, (b) HAZ, and (c) base metal*

The microstructure images of specimen 125-2 (Fig. 8) reveal variations in the quantity and arrangement of ferrite and pearlite in the weld metal, HAZ, and base metal regions. The pearlite phase is more prevalent than the ferrite phase in the weld metal region (Fig. 8a). A similar occurrence is observed in the heat-affected zone (HAZ) area, as shown in Fib. 8b. In Fig. 8c, the base metal area exhibits a significant prevalence of the ferrite phase compared to the weld metal and heat-affected zone (HAZ) sections. A predominance of the pearlite phase often characterizes the regions of the weld metal and heat-affected zone (HAZ). The presence of ferrite phase was observed in both the weld metal and heat-affected zone (HAZ), with a minimal quantity and tiny dimensions. In general, the weld metal area exhibits the maximum hardness level, with the heat-affected zone (HAZ) following closely behind. The base metal area has the lowest hardness due to its higher proportion of ferrite than pearlite.
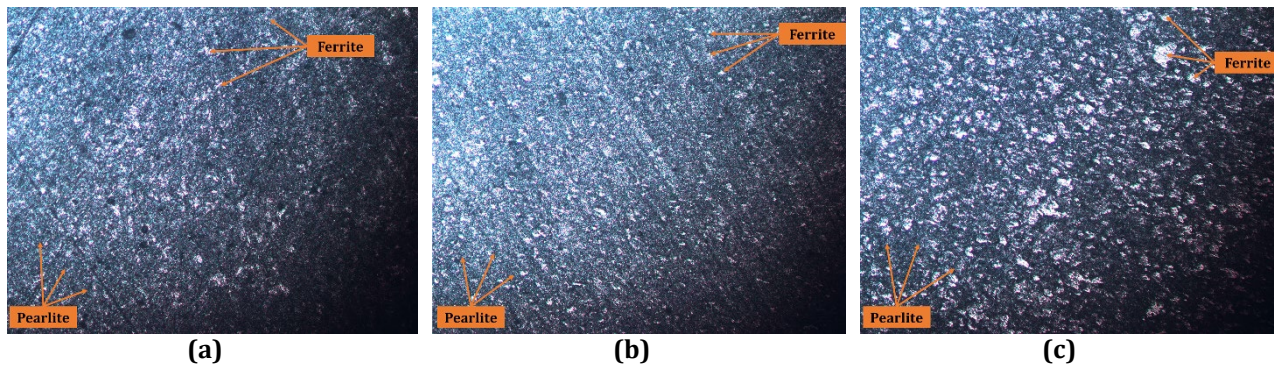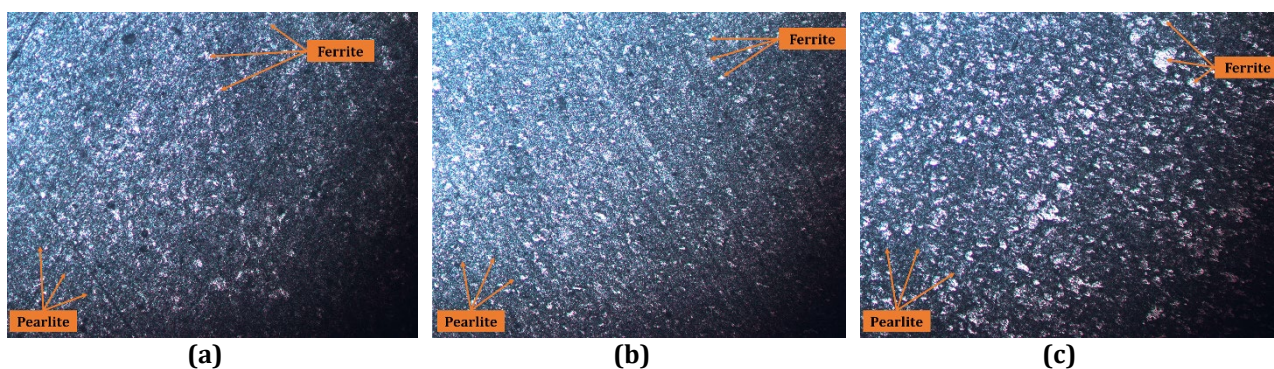
**Fig. 8** *Microstructure of the 125-2 specimen: (a) weld metal, (b) HAZ, and (c) base metal.*
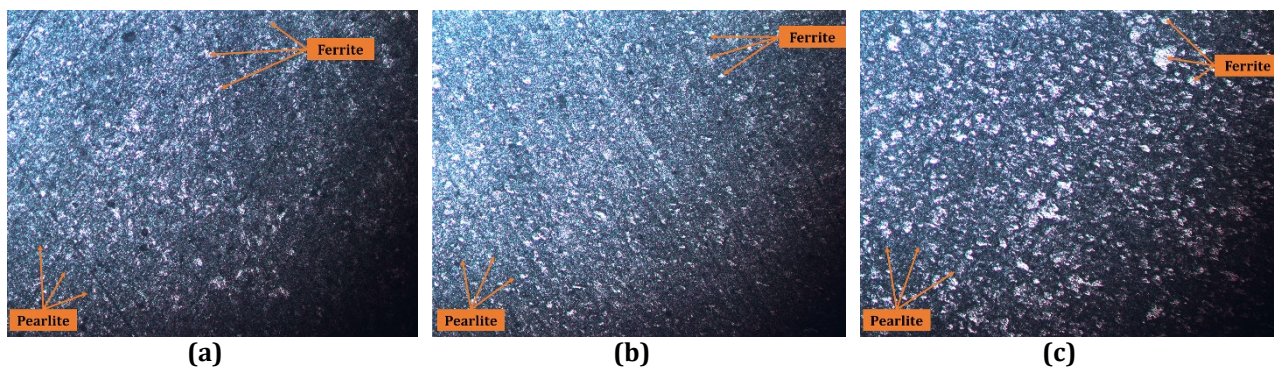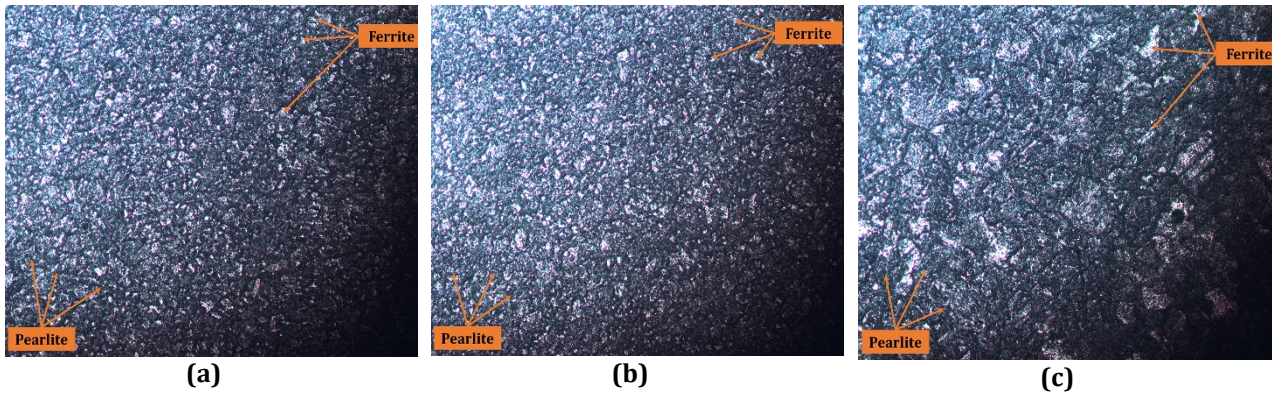


**Fig. 9** *Microstructure of the 135-2 specimen: (a) weld metal; (b) HAZ; (c) base metal*

In specimen 135-2 (Fig. 9a), the microstructure of the weld metal is characterized by the prevalence of pearlite phase grains, which appear as solid black. Conversely, the ferrite phase, which is dazzling white, is present in limited quantities in this region. In specimen 135-2, the HAZ area (Fig. 9b) included ferrite with a greater abundance and larger size than the ferrite detected in the weld metal area. This decreases hardness in the heat-affected zone (HAZ) compared to the weld metal region. The base metal area (Fig. 9c) exhibits a distinct structure compared to the weld metal and heat-affected zone (HAZ) sections. The image microstructure analysis reveals a higher abundance of ferrite phases in the base metal region compared to the weld metal and heat-affected zone (HAZ) regions. The predominance of the ferrite phase in the microstructure of the base metal results in the base metal area exhibiting soft and ductile characteristics.



**Fig. 10** *Microstructure of the 145-2 specimen: (a) weld metal; (b) HAZ; (c) base metal*

Fig. 10 displays microstructure images of specimen 145-2. The microstructure analysis reveals the existence of ferrite and pearlite in the weld metal, heat-affected zone (HAZ), and base metal regions. The three photos depict variations in the composition and quantity in each area. The amount of pearlite present in the weld metal region (Fig. 10a) is more significant compared to the heat-affected zone (Fig. 10b) and the base metal (Fig. 10c). In the base metal region, the quantity of ferrite exceeds that of pearlite. A uniform distribution of ferrite, which is small and bright white in color, is readily apparent in the region containing the base metal. This is distinct from that found in the weld metal area, which frequently contains just a small amount of ferrite phase. The microstructure explains that the weld metal area exhibits the highest hardness value while the base metal area displays the lowest.

**Fig. 11** *Microstructure of the 155-2 specimen: (a) weld metal; (b) HAZ; (c) base metal*

Figures 11a, 11b, and 11c display the microstructures of the weld metal, heat-affected zone (HAZ), and base metal areas of specimen 155-2, respectively. The obtained microstructure reveals differences in the quantity and arrangement of ferrite and pearlite phases. The weld metal area exhibits a significant increase in the quantity of pearlite and a reduction in ferrite. The heat-affected zone (HAZ) exhibits the same phase as the weld metal area. However, it contains a higher ferrite concentration than the weld metal area. In contrast to the weld metal and HAZ areas, the base metal region predominantly comprises ferrite phases, resulting in a relatively low hardness value compared to the aforementioned areas.
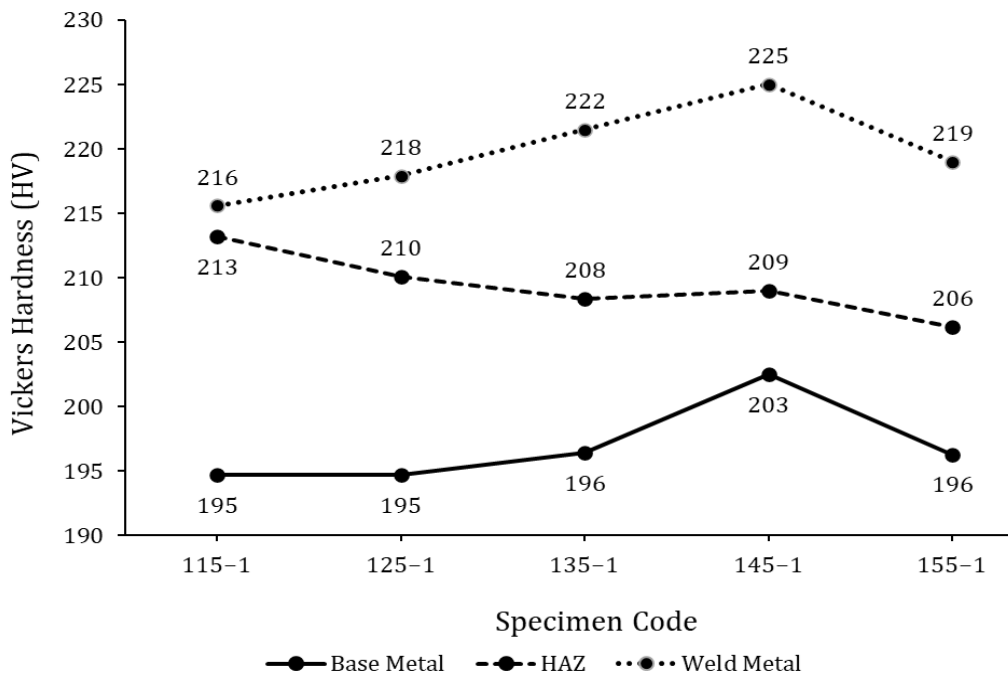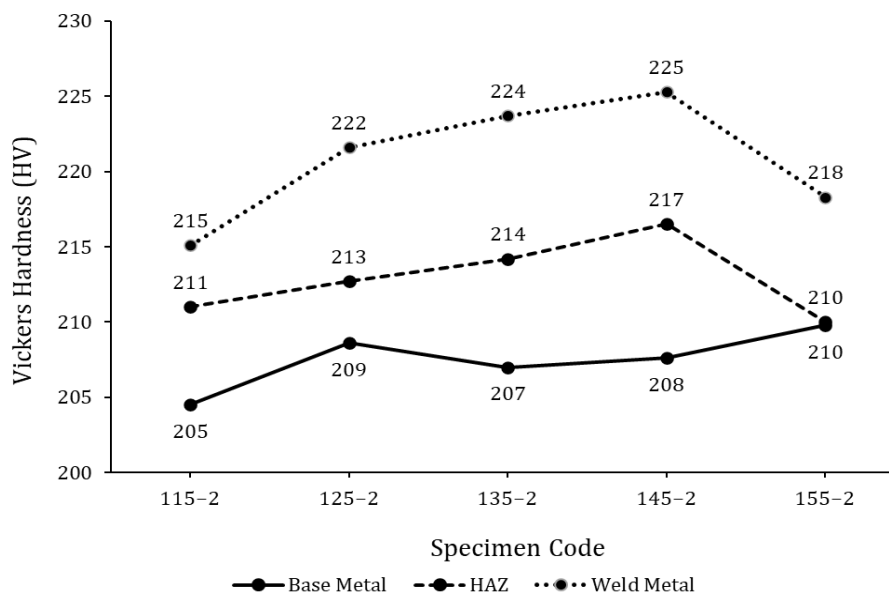


**Fig. 12** *Hardness of specimens before finishing*

The hardness of the specimens before and after finishing is illustrated in Fig. 12 and Fig. 13. The weld metal area typically exhibits greater hardness than the base metal and heat-affected zone (HAZ) portions. All variations of welding current utilized for hardfacing treatment exhibit this characteristic on specimens both before and after the finishing process. This aligns with the findings from the analysis of the microstructure. The region within the weld metal where pearlite is more prevalent than ferrite. Consequently, an area with increased hardness is generated. According to research conducted by Li et al. (2020) [36], the hardness of welded materials can be influenced by various factors. Significant factors are the composition and type of filler metal utilized during the welding procedure. An illustration of this can be seen in the weld metal composition when carbon steel is employed as the filler metal. Typically, the weld metal comprises pearlite and ferrite. Furthermore, martensite formation can occur during the transition from a stainless-steel weld to a carbon steel weld due to the elevated carbon and alloying element contents. The presence of martensite phases in the weld metal could result in an enhancement of its hardness. The welding process parameters, including the input of heat, cooling rate, and

Penerbit
UTHM

welding speed, are additional factors that might impact the mechanical characteristics and microstructure of the weld metal. The heat input and cooling rate can influence the creation of various phases in the weld metal, such as martensite, as well as the distribution of grain size and microstructure. The velocity at which welding is performed can impact the pace at which the material cools down and the quantity of heat that is applied, thereby influencing the mechanical properties and microstructure of the welded metal. The increased hardness of the weld metal compared to the base metal can be attributed to the creation of the martensite phase within the weld metal [36].

The findings of this study demonstrate that the hardness of the final specimens is influenced by the hardfacing process conducted with different current variations. This is evidenced by the different levels of hardness observed in each acquired specimen. Differences in the welding current employed during the hardfacing procedure will result in varying hardness levels in each specimen. This occurs due to the fact that the heat input during the welding process is influenced by the welding current. The weld metal undergoes hardness due to the heat distribution that takes place during the welding process. The welding process generates high temperatures through the use of electric current. As the current increases, the heat input also increases. This leads to an extended period of cooling, which has a direct effect on the final shape of the phase.

The weld metal might undergo hardening due to alterations in its chemical composition and crystal structure produced by the heat generated during welding. Uneven heat distribution can cause the transformation of the austenitic structure to martensite and pearlitic, thereby increasing the hardness of the weld metal. According to a study by Amosun et al. (2023) [37], the increase in hardness in the weld metal region was the result of a high heat input that transformed the microstructure and prevented it from returning to its original form due to the rapid cooling process. The transformation of the microstructure to martensite results in an increase in the hardness of the weld metal [37]. According to studies conducted by Köse (2022) [38] and Roy et al. (2022) [39], an excessive amount of heat input will decrease the strength and hardness of the specimen.



**Fig. 13** *Hardness of specimens after finishing*

The findings of this study suggest that the welding current employed will enhance the hardness of both the weld metal and base metal in the specimen before finishing (Fig. 12). This behaviour becomes evident when the welding current is raised from 115A to 145A. Nevertheless, welding currents over 145 A substantially reduced the hardness of both the weld metal and base metal. The same was observed for specimens that had undergone the finishing process (Fig. 13). The weld metal hardness of the final samples exhibited a direct correlation with the welding current, which ranged from 115A to 145A. Nevertheless, if the welding current is higher than 145 A, there is a notable reduction in the hardness of the weld metal. The results of this study suggest that increasing the welding current employed during the hardfacing process does not significantly change the hardness in the heat-affected zone (HAZ) area. The analysis results in this study show that the weld metal has the highest hardness level in specimens that experience hardfacing with a welding current of 145 A, both before and after finishing, with a resulting hardness of 225 HV. In the meantime, the weld metal with the lowest hardness is observed in specimens that were hardfaced with a welding current of 115 A, followed by a finishing treatment of 215 HV. Asibeluo et al. (2015) investigated the influence of increased welding current on the hardness reduction in weld joints composed of A36 carbon steel. According to their study, the heat input in A36 carbon steel welded connections increased when the welding current was raised from 70A to 120A. This affects the weld's

microstructure and decreases the impact strength and hardness of the welded metal. The application of a welding current of 120A results in a reduction in grain size, thereby influencing the specimen's hardness and durability [40]. Consistent results were also discovered in a study published by Syukran et al. (2022). According to their study, enhancing the welding current from 80A to 100A results in a 1.2% decrease in the weld metal hardness value, from 42.3 HRC to 41.8 HRC. In addition, a 14.7% reduction in hardness is observed when the current is increased from 100A to 120A, from 41.8 HRC to 35.7 HRC [41]. According to research conducted by Vietanti et al. (2021), the hardness of weld metal on the ASTM A36 steel plate decreases as the current increases. This is because as the grains become coarser, their hardness diminishes [42]. Singh et al. (2020) conducted research utilizing shielded metal arc welding at currents of 425, 450, and 475 A. According to their investigation, the hardness (HRB) values obtained by welding at currents of 425, 450, and 475 A were 75.4, 72.1, and 70.9, respectively. As the current employed increases, the resultant hardness decreases [43]. The findings presented in this study align with the research conducted by Tahir et al. (2018). Tahir et al. (2018) found that raising the welding current from 80A to 90A decreased the average Rockwell hardness from 34.8 HRC to 32.2 HRC. This is the result of an increase in welding current and heat input, which reduces the hardness of the welded material [44].

## 4. Conclusions

The hardfacing process on the timing pulley shaft has been successfully executed utilizing the shielded metal arc welding (SMAW) method. The timing pulley shaft in this study was manufactured using AISI 1045 medium carbon steel, with a hardness of 213 HV and a predominant ferrite phase in its microstructure. The research findings suggest that the hardness of the specimen is affected by the application of electric current during the hardfacing process. This is evidenced by the differences in the observed hardness levels of each obtained specimen. As the welding current rises, so does the heat input. Unequal thermal dispersion can lead to the transformation of the austenitic structure into pearlitic, thereby enhancing the hardness of the welded metal. Higher pearlite content leads to increased hardness.

According to this study, raising the welding current from 115 A to 145 A will result in a consistent increase in the hardness of the weld metal across all samples. Nevertheless, welding currents that exceed 145 A noticeably diminish the hardness of the weld metal. The weld metal exhibiting the greatest level of hardness was observed in specimens subjected to hardfacing with a welding current of 145 A. The hardness of the weld metal, HAZ, and base metal in specimens treated with hardfacing at a current of 145 A (before finishing) was 225 HV, 209 HV, and 203 HV, respectively. After finishing, the hardness of this specimen's weld metal, HAZ, and base metal was 225 HV, 217 HV, and 208 HV, respectively. The weld metal with the lowest hardness (215 HV) is discovered in specimens that were hardfaced with a welding current of 115 A and finished. The weld metal's hardness in this study exhibited a negative correlation with the current's magnitude.

## Acknowledgement

## Conflict of Interest

Authors declare that there is no conflict of interests regarding the publication of the paper.

## Author Contribution

*The authors confirm contribution to the paper as follows: **study conception and design:** Basyirun Basyirun, Muhammad Hasnan Habib; **data collection:** Deni Fajar Fitriyana, Muhammad Irfan Nuryanta; **analysis and interpretation of results:** Januar Parlaungan Siregar, Tezara Cionita, Natalino Fonseca Da Silva Guterres; **draft manuscript preparation:** Mateus De Sousa Da Silva, Basyirun Basyirun. All authors reviewed the results and approved the final version of the manuscript.*

## References

[1]  Cui, P., Zhang, Y., & Xue, Y. (2020). A novel method of analyzing spinning tensions for yarn breakage detection in ring frame. Journal of Engineered Fibers and Fabrics, 15, 1558925020902979. https://doi.org/10.1177/1558925020902979

[2]  Tchomeni Kouejou, B. X., & Alugongo, A. A. (2023). Experimental Analysis of a Cracked Cardan Shaft System under the Influence of Viscous Hydrodynamic Forces. In Fluids (Vol. 8, Issue 7). https://doi.org/10.3390/fluids8070211

[3]  Childs, P. R. N. (2014). Chapter 7 - Shafts (P. R. N. B. T.-M. D. E. H. Childs (ed.); pp. 255–315). Butterworth-Heinemann. https://doi.org/https://doi.org/10.1016/B978-0-08-097759-1.00007-1

[4] Tandon, D., Li, H., Pan, Z., Yu, D., & Pang, W. (2023). A Review on Hardfacing, Process Variables, Challenges, and Future Works. In Metals (Vol. 13, Issue 9). https://doi.org/10.3390/met13091512

[5] Venkatesh, B., Anil Kumar Reddy, C., & Raghupathi. (2022). Tribological Characteristics of Stellite Hard faced Layer on Mild Steel. IOP Conference Series: Materials Science and Engineering, 1248(1), 012039. https://doi.org/10.1088/1757-899x/1248/1/012039

[6] Balaguru, S., & Gupta, M. (2021). Hardfacing studies of Ni alloys: a critical review. Journal of Materials Research and Technology, 10, 1210–1242. https://doi.org/https://doi.org/10.1016/j.jmrt.2020.12.026

[7] Naboychenko, S. S., Murashova, I. B., & Neikov, O. D. (2009). Chapter 17-Production of nickel and nickel-alloy powders carbonyl process of nickel powder. In Handbook of non-ferrous metal powders (pp. 369–398). https://doi.org/10.1016/B978-1-85617-422-0.00017-3

[8] Nagentrau, M., Tobi, A. L. M., Sambu, M., & Jamian, S. (2019). The influence of welding condition on the microstructure of WC hardfacing coating on carbon steel substrate. International Journal of Refractory Metals and Hard Materials, 82, 43–57. https://doi.org/https://doi.org/10.1016/j.ijrmhm.2019.03.029

[9] Jankauskas, V., Antonov, M., Varnauskas, V., Skirkus, R., & Goljandin, D. (2015). Effect of WC grain size and content on low stress abrasive wear of manual arc welded hardfacings with low-carbon or stainless steel matrix. Wear, 328–329, 378–390. https://doi.org/https://doi.org/10.1016/j.wear.2015.02.063

[10] Alipooramirabad, H., Paradowska, A., Ghomashchi, R., & Reid, M. (2017). Investigating the effects of welding process on residual stresses, microstructure and mechanical properties in HSLA steel welds. Journal of Manufacturing Processes, 28, 70–81. https://doi.org/https://doi.org/10.1016/j.jmapro.2017.04.030

[11] Fei, Z., Pan, Z., Cuiuri, D., Li, H., Wu, B., & Su, L. (2019). Improving the weld microstructure and material properties of K-TIG welded armour steel joint using filler material. International Journal of Advanced Manufacturing Technology, 100(5–8), 1931–1944. https://doi.org/10.1007/s00170-018-2787-y

[12] Sreeraj, P., Kannan, T., & Maji, S. (2013). Simulation and Parameter Optimization of Gmaw Process Using Neural Networks and Particle Swarm Optimization Algorithm. Int. J. Mech. Eng. & Rob. Res, 2(1). www.ijmerr.com

[13] Lakshminarayanan, A. K., Balasubramanian, V., & Elangovan, K. (2009). Effect of welding processes on tensile properties of AA6061 aluminium alloy joints. International Journal of Advanced Manufacturing Technology, 40(3–4), 286–296. https://doi.org/10.1007/s00170-007-1325-0

[14] Suharno, Fikri, M. R., Pambudi, N. A., Harjanto, B., Jumintono, & Rizkiana, R. (2023). The effect of variation of the electric current on physical and mechanical properties in A36 steel welding. Welding International, 37(10), 553–562. https://doi.org/10.1080/09507116.2023.2264175

[15] Singh, S., Kumar, R., Goel, P., & Singh, H. (2022). Analysis of wear and hardness during surface hardfacing of alloy steel by thermal spraying, electric arc and TIG welding. Materials Today: Proceedings, 50, 1599–1605. https://doi.org/https://doi.org/10.1016/j.matpr.2021.09.122

[16] Singh, R. (2016). Chapter 6 - Classification of Steels. In R. B. T.-A. W. E. (Second E. Singh (Ed.), Applied Welding Engineering (Second Edition) (pp. 57–64). Butterworth-Heinemann. https://doi.org/https://doi.org/10.1016/B978-0-12-804176-5.00006-2

[17] Dossett, J. L. (2020). Chapter 5: Classification of Carbon and Low-Alloy. In ASM TECHNICAL BOOKS Practical Heat Treating: Basic Principles (pp. 95–126). https://doi.org/10.31399/asm.tb.phtbp.t59310095

[18] Gao, K., Qin, X., Wang, Z., & Zhu, S. (2016). Effect of spot continual induction hardening on the microstructure of steels: Comparison between AISI 1045 and 5140 steels. Materials Science and Engineering: A, 651, 535–547. https://doi.org/https://doi.org/10.1016/j.msea.2015.11.012

[19] Abbas, A. T., Benyahia, F., El Rayes, M. M., Pruncu, C., Taha, M. A., & Hegab, H. (2019). Towards Optimization of Machining Performance and Sustainability Aspects when Turning AISI 1045 Steel under Different Cooling and Lubrication Strategies. In Materials (Vol. 12, Issue 18). https://doi.org/10.3390/ma12183023

[20] Wardani, I. P., Setyowati, V. A., Suheni, S., & Samudra, I. P. (2020). the Effect of Welding Current on Aisi 1045 Strength and Corrosion Rate. Journal of Applied Sciences, Management and Engineering Technology, 1(2), 40–45. https://doi.org/10.31284/j.jasmet.2020.v1i2.1159

[21] Triantoro, TBW, Waluyo, M. (2023). Metoga GTAW Welding Joint Strength Study For Aisi 1045 Application Of Milling Tools. PENA TEKNIK: Jurnal Ilmiah Ilmu-Ilmu Teknik, 8(1), 10–19. https://doi.org/10.51557/pt_jiit.v8i1.1688

[22] Moore, P., & Booth, G. (2015). 9 - Mechanical testing of welds. In P. Moore & G. B. T.-T. W. E. G. to F. and F. Booth (Eds.), The Welding Engineers Guide to Fracture and Fatigue (pp. 113–141). Woodhead Publishing. https://doi.org/https://doi.org/10.1533/9781782423911.2.113

[23] Buitrago Diaz, J. C., Ortega-Portilla, C., Mambuscay, C. L., Piamba, J. F., & Forero, M. G. (2023). Determination of Vickers Hardness in D2 Steel and TiNbN Coating Using Convolutional Neural Networks. In Metals (Vol. 13, Issue 8). https://doi.org/10.3390/met13081391

[24] Polanco, J. D., Jacanamejoy-Jamioy, C., Mambuscay, C. L., Piamba, J. F., & Forero, M. G. (2023). Automatic Method for Vickers Hardness Estimation by Image Processing. In Journal of Imaging (Vol. 9, Issue 1). https://doi.org/10.3390/jimaging9010008

[25] Cheng, W.-S., Chen, G.-Y., Shih, X.-Y., Elsisi, M., Tsai, M.-H., & Dai, H.-J. (2022). Vickers Hardness Value Test via Multi-Task Learning Convolutional Neural Networks and Image Augmentation. In Applied Sciences (Vol. 12, Issue 21). https://doi.org/10.3390/app122110820

[26] Sofyan, D., Badri, M., Dalil, M., Reforiandi, A., & Surya, A. (2020). Calibration of Vickers Hardness Test Equipment Using Standard Block ( Case study in PT . Tenaris SPIJ , Cilegon ). Journal of Ocean, Mechanical and Aerospace, 64(3), 81–87. http://dx.doi.org/10.36842/jomase.v64i3.203

[27] American Welding Society. (2002). AWS/SAE D8.9M, Recommended Practices for Test Methods for Evaluating the Resistance Spot Welding Behavior of Automotive Sheet Steel Materials. 1–9. https://pubs.aws.org/Download_PDFS/d8.9mPV.pdf

[28] Zhu, X., Zhu, Y., Kang, C., Liu, M., Yao, Q., Zhang, P., Huang, G., Qian, L., Zhang, Z., & Yao, Z. (2023). Research on Automatic Identification and Rating of Ferrite&ndash;Pearlite Grain Boundaries Based on Deep Learning. In Materials (Vol. 16, Issue 5). https://doi.org/10.3390/ma16051974

[29] Gadalińska, E., Baczmański, A., Braham, C., Gonzalez, G., Sidhom, H., Wroński, S., Buslaps, T., & Wierzbanowski, K. (2020). Stress localisation in lamellar cementite and ferrite during elastoplastic deformation of pearlitic steel studied using diffraction and modelling. International Journal of Plasticity, 127, 102651. https://doi.org/https://doi.org/10.1016/j.ijplas.2019.102651

[30] Eiken, J., Böttger, B., & Apel, M. (2023). Diffuse modelling of pearlite growth in Calphad-coupled multicomponent multi-phase-field simulations. IOP Conference Series: Materials Science and Engineering, 1281(1), 012051. https://doi.org/10.1088/1757-899x/1281/1/012051

[31] Ruggiero, A., & Khademi, E. (2023). Micromechanical Modeling for Predicting Residual Stress&ndash;Strain State around Nodules in Ductile Cast Irons. In Metals (Vol. 13, Issue 11). https://doi.org/10.3390/met13111874

[32] Arshad, W., Mehmood, A., Hashmi, M. F., & Rauf, O. U. (2018). The Effect of Increasing Silicon on Mechanical Properties of Ductile Iron. Journal of Physics: Conference Series, 1082(1). https://doi.org/10.1088/1742-6596/1082/1/012059

[33] Duka, E., Oettel, H., & Dilo, T. (2012). Connection between micro and macro hardness pearlitic-ferritic steel. AIP Conference Proceedings, 1476(May), 47–51. https://doi.org/10.1063/1.4751563

[34] Torbati-Sarraf, H., & Poursaee, A. (2020). The influence of phase distribution and microstructure of the carbon steel on its chloride threshold value in a simulated concrete pore solution. Construction and Building Materials, 259, 119784. https://doi.org/https://doi.org/10.1016/j.conbuildmat.2020.119784

[35] Tonizzo, Q., Caillard, D., Perlade, A., Mazière, M., & Gourgues-Lorenzon, A. F. (2019). Multiscale examination of deformation and fracture mechanisms of a duplex advanced high strength steel: Effect of testing temperature and of micromechanical interactions between microstructural constituents. Materials Science and Engineering: A, 764, 138196. https://doi.org/https://doi.org/10.1016/j.msea.2019.138196

[36] Li, C., Qin, G., Tang, Y., Zhang, B., Lin, S., & Geng, P. (2020). Microstructures and mechanical properties of stainless steel clad plate joint with diverse filler metals. Journal of Materials Research and Technology, 9(2), 2522–2534. https://doi.org/10.1016/j.jmrt.2019.12.083

[37] Amosun, T. S., Hammed, S. O., de Lima, A. M. G., & Habibi, I. (2023). Effect of quenching media on mechanical properties of welded mild steel plate. Mechanical Engineering for Society and Industry, 3(1), 3–11. https://doi.org/10.31603/mesi.7121

[38] Köse, C. (2022). Effect of heat input and post weld heat treatment on the texture, microstructure and mechanical properties of laser beam welded AISI 317L austenitic stainless steel. Materials Science and Engineering: A, 855(143966), 1–34. https://doi.org/https://doi.org/10.1016/j.msea.2022.143966

[39] Roy, A., Ghosh, N., & Mondal, S. (2023). Effect of heat input on mechanical and metallurgical properties of AISI 304L stainless steel by using TIG welding. Welding International, 37(2), 91–100. https://doi.org/10.1080/09507116.2023.2185169

[40] Asibeluo, I. S., & Emifoniye, E. (2015). Effect of Arc Welding Current on the Mechanical Properties of A36 Carbon Steel Weld Joints. International Journal of Mechanical Engineering, 2(9), 32–40. https://doi.org/10.14445/23488360/ijme-v2i9p113

[41] Syukran, S., & Azwinur, A. (2022). Hardness Analysis of Weld Metal Electrode Low Hydrogen Potassium E7016 and E7018. Journal of Welding Technology, 4(2), 44–47. https://doi.org/10.30811/jowt.v4i2.3492

[42] Vietanti, F., Rajan, A. F., Arifin, A. A., Feryanto, D. H., Suheni, Irawan, H., Ulum, M., Arif, R. Z., Dicky, M. A., & Darmawan, F. B. (2021). Analysis of Welding Position and Current on Mechanical Properties of A36 Steel using Shield Metal Arc Welding. Journal of Physics: Conference Series, 2117(1). https://doi.org/10.1088/1742-6596/2117/1/012001

[43] Singh, R. P., Singh, A., & Singh, A. (2019). Optimization of hardness of weld in submerged arc welding. Materials Today: Proceedings, 26(xxxx), 1827–1830. https://doi.org/10.1016/j.matpr.2020.02.382

[44] Tahir, A. M., Lair, N. A. M., & Wei, F. J. (2018). Investigation on mechanical properties of welded material under different types of welding filler (shielded metal arc welding). AIP Conference Proceedings, 1958, 1–7. https://doi.org/10.1063/1.5034534